Waste Management Bulletin 2 (2024) 327–339

Contents lists available at ScienceDirect

Waste Management Bulletin

journal homepage: www.elsevier.com/locate/wmb

Green synthesis of gaharu leaf extract-modified magnetite as an adsorbent for methyl orange textile dyes

Triastuti Sulistyaningsih [a,*], Dwi Atika Sari [a], Nuni Widiarti [a], Widi Astuti [b], Rika Wulandari [c], Dewanto Harjunowibowo [d]

[a] Chemistry Department, Universitas Negeri Semarang, Sekaran, Gunungpati 50229, Jawa Tengah, Indonesia
[b] Chemical Engineering Department, Universitas Negeri Semarang, Sekaran, Gunungpati 50229, Jawa Tengah, Indonesia
[c] Research Center for Pharmaceutical Ingredient and Traditional Medicine, Research Organization for Health, Badan Riset dan Inovasi Nasional (BRIN), Cibinong, Bogor, Jawa Barat, Indonesia
[d] Physics Education Department, Universitas Sebelas Maret, Surakarta, Jawa Tengah, Indonesia

ARTICLE INFO

Keywords:
Green synthesis
Gaharu leaf extract
Magnetite
Adsorbent
Methyl orange

ABSTRACT

Magnetite, a widely synthesized compound utilized as an adsorbent in various processes, exhibits reduced adsorption efficiency due to aggregation in aqueous solutions. Addressing this limitation, modification of magnetite is necessary to mitigate agglomeration and enhance adsorption capacity. Herein, we propose the utilization of gaharu leaf extract for magnetite modification, leveraging its abundance as a byproduct of essential oil production and rich secondary metabolite content, which serves as a stabilizing agent in synthesis processes. Magnetite (M) and gaharu leaf extract-modified magnetite (MEDG) were synthesized and evaluated as adsorbents for methyl orange (MO) textile dyes. Characterization via FTIR, PSA, SEM-EDX, XRD, and VSM revealed distinctive features of MEDG, including vibrational peaks corresponding to organic functional groups derived from the secondary metabolites present in the gaharu leaf extract. These functional groups actively participate in the adsorption process and prevent magnetite aggregation. MEDG exhibited a particle size of 4408.7 nm, compared to 4625 nm for M, with both exhibiting face-centered cubic (fcc) crystal structures. Additionally, MEDG demonstrated a crystallinity percentage of 92.49 % and saturation magnetization of 34.43 emu/g, attributed to the incorporation of gaharu leaf extract. Adsorption studies demonstrated that MEDG and gaharu leaf simplicia (SDG) achieved maximal adsorption of MO at pH 3 for 60 min and pH 4 for 70 min, respectively, with an adsorption efficiency of 95–99 % for a 5 ppm MO solution. The adsorption kinetics followed Ho's pseudo-second-order model, and the isotherm conformed to Freundlich's model. Furthermore, M and MEDG exhibited high reusability, with up to 5 cycles of reuse, while SDG demonstrated 3 cycles. However, the adsorption efficiency decreased to 87 % for MEDG and 85.19 % for SDG upon the fifth repetition. In conclusion, modification of magnetite with gaharu leaf extract enhances its adsorption capacity, offering economic advantages over pure magnetite due to increased surface area and active sites.

Introduction

Textile dye waste poses a challenge for decomposition due to containing carcinogenic azo groups (Oyetade et al., 2022). Various methods have been utilized to mitigate textile dye waste in the industry, including adsorption (Al-husseiny and Ebrahim, 2022; Astuti et al., 2017; El-kammah et al., 2022; Sulistyaningsih et al., 2016), photocatalytic (Hashmi et al., 2021), electrocoagulation (Tones et al., 2020), and Fenton oxidation (Masalvad and Sakare, 2020). Adsorption is favored due to its ease of implementation and minimal production of toxic waste (de Oliveira et al., 2023), involving the attachment of an adsorbent to the surface of an adsorbate due to attractive forces.

Previous studies have explored methyl orange (MO) adsorption using various materials, including Co_3O_4, but reported limited adsorption capacities relative to the mass of adsorbent used. For instance, Uddin and Baig (2019) found that only 46.08 ppm of MO compound was adsorbed using 500 mg of adsorbent in 50 mL of 50 ppm MO solution. Another study by Hussain et al. (2021) investigated MO adsorption

* Corresponding author.
E-mail address: triastuti.s@mail.unnes.ac.id (T. Sulistyaningsih).

https://doi.org/10.1016/j.wmb.2024.02.007

Available online 2 March 2024

using a chitosan-zeolite film, which absorbed 173 ppm of MO solution with an initial concentration of 327 ppm using 100 mg of adsorbent. However, the amount of MO adsorbed remains relatively low compared to the mass of adsorbent used, prompting this research to evaluate the adsorption ability of magnetite to absorb MO solution, with the expectation that magnetite modified with gaharu leaf extract (MEDG) will exhibit superior adsorption capacity.

Magnetite is commonly used in adsorption processes, including for textile dyes, but can suffer from agglomeration in aqueous solutions, leading to decreased adsorption ability (Mohammadzadeh and Leiviskä, 2023). Hence, magnetite requires modification to enhance its adsorption capacity, which can be achieved by adding natural ingredients (Altaf et al., 2021; Mohammadzadeh and Leiviskä, 2023; Rahmayanti et al., 2022), oleic acid (Masuku et al., 2021), phosphate (Masuku et al., 2021), humic acid (Ahmad et al., 2022; Sulistyaningsih et al., 2021), or hydrotalcite (Sulistyaningsih et al., 2013). These additions aim to increase active sites and prevent agglomeration.

Among various magnetite modifications, plant extracts are commonly used. Several plants have been employed for this purpose, including Moringa olifera leaves (Altaf et al., 2021), guava leaves (Rusmana and Sulistyaningsih, 2021), *Peltophorum pterocarpum* pods (Dash et al., 2019), *Excoecaria cochinchinensis* leaves (Cai et al., 2019), pistachio leaves (*Pistacia vera*) (Tamoradi and Mousavi, 2020), *Plantago major* leaves (Lohrasbi et al., 2019), *Azadirachta indica* leaves (Maheswari and Reddy, 2016), *Averrhoa carambola* leaves (Padhi et al., 2017), *Dolichos lablab* pods (Basavaiah et al., 2018), and jengkol (*Archidendron pauciflorum*) peel (Rahmayanti et al., 2022). These modifications have demonstrated adsorption efficiency values of around 80–90 %, and they aim to increase active sites and ensure that secondary metabolite compounds in the natural material adhere to the magnetite surface (Altaf et al., 2021; López and Antuch, 2020; Rahmayanti et al., 2022), thereby enhancing adsorption ability.

Extracts from natural ingredients contain various compounds, including amino acids, polyphenols, nitrogen bases, and reducing sugars, as well as functional groups like hydroxyl, ether, carbonyl, and carboxyl groups (López and Antuch, 2020; Rahmayanti et al., 2022). These compounds serve as stabilizing agents during the synthesis of magnetite (López and Antuch, 2020; Mittal et al., 2013). Moreover, these functional groups can act as active sites on the surface of magnetite, enhancing its ability to adsorb textile dyes effectively. The synthesis of magnetite using plant extracts is referred to as green synthesis (Altaf et al., 2021), aligning with the principles of green chemistry.

Green synthesis offers several advantages, including energy and cost savings, environmental friendliness, and reduced negative impacts of chemical production (Das et al., 2014; Saif et al., 2016). The addition of gaharu (*Aquilaria malaccensis* Lam.) leaf extract to magnetite for modification exemplifies a green synthesis approach. Gaharu trees are adaptable to various conditions and soil types, particularly thriving in open fields (Huda et al., 2015). Gaharu leaves, often discarded as waste in the essential oil industry, contain compounds that can enhance adsorption efficiency. Comparatively, gaharu leaf extract has been found to have higher flavonoid, tannin, and alkaloid content than Moringa oleifera leaf extract, indicating a potential increase in adsorption efficiency with gaharu leaf extract modification.

The addition of gaharu leaf extract is expected to enhance the adsorption efficiency of magnetite due to its higher flavonoid, tannin, and alkaloid content compared to the previously used extract. Gaharu leaf extract contains 8.34, 5.63, and 7.2 % flavonoid, tannin, and alkaloid levels, respectively (Gama et al., 2021; Septiani et al., 2018). Furthermore, gaharu leaves have a higher phenolic compound content, with 14.81 %, compared to Moringa oleifera leaves, which have only 2.28 % (Sankhalkar and Vernekar, 2016; Septiani et al., 2018). In comparison with other plants, gaharu also contains higher levels of flavonoids, tannins, alkaloids, and phenolics.

Previous studies have shown that magnetite modification with Moringa oleifera leaves resulted in good adsorption and reusability capabilities, with an adsorption efficiency of around 80–85 % after four repetitions. Given the higher organic compound content in gaharu leaves, it is expected that adsorption efficiency and reusability will be even higher than those of magnetite modified with Moringa oleifera leaves. Additionally, Moringa oleifera leaves are widely used as a food ingredient, while gaharu leaves are not as commonly utilized. Utilizing gaharu leaves, which are waste from the essential oil industry, is therefore important to prevent them from becoming waste.

In the application of MEDG as an adsorbent for MO textile dyes, it is important to compare its efficiency with M and SDG to determine its superiority. This comparison will help evaluate whether magnetite modified with gaharu leaf extract has significantly higher adsorption ability than M and SDG. Studying the adsorption capacity of MEDG is also crucial to assess its feasibility for industrial-scale application.

Recent studies have shown that composite materials have been widely developed as adsorbents in the last five years (Iwuozor et al., 2021; Sulistyaningsih et al., 2013). Composites are synthesized to enhance the adsorption capacity of various materials, making them more effective than activated carbon. While the production of activated carbon requires high temperatures and longer processing times, the synthesis of magnetite is relatively quicker and requires lower temperatures (Ahmad et al., 2024). The precursor for magnetite synthesis is also inexpensive, and the concentration required is lower than that for activated carbon activation (Astuti et al., 2020, 2023; Kosheleva et al., 2019). The washing or neutralization process for magnetite is also shorter due to its easy settling, allowing for quicker leaching at a neutral pH. Therefore, modified magnetite with natural ingredients, specifically gaharu leaf extract, has the potential to be developed and applied on an industrial scale.

Materials and method

Materials

The materials employed in this study included iron(II) sulfate heptahydrate, iron(III) chloride hexahydrate, sodium hydroxide, hydrochloric acid, magnesium powder, and methyl orange, all sourced from Merck. Dragendorf's reagent, ethanol, and distilled water were also essential for the experiments. The gaharu leaves were sourced from a plantation in the Gunungpati area, Semarang.

Gaharu leaf extract preparation

Gaharu leaves were washed with distilled water and dried at 50 °C for 12 h in an oven. The dried leaves were then pulverized and homogenized to a uniform size using a 50-mesh sieve. Subsequently, 10 g of the pulverized leaves were macerated with 100 mL of ethanol for three consecutive 24-hour periods. The maceration process occurred in a light-free environment, with the mixture being stirred every 8 h for 30 s. Following maceration, the filtrate was separated from the residue through filtration to obtain the gaharu leaf extract.

To test the extract's phytochemical composition, 2 mL of the gaharu leaf extract was diluted with 2 mL of distilled water and divided into four test tubes. The first tube received HCl solution and magnesium

powders. The presence of flavonoids was indicated by an orange or red color change. The second tube received NaCl and iron(III) chloride solution, with a dark green color indicating the presence of tannin compounds. Dragendorf's reagent was added to the third tube, and an orange color change indicated the presence of alkaloid compounds. The fourth tube served as a control to observe any color changes before and after phytochemical testing.

Synthesis of magnetite (M)

Iron(II) sulfate heptahydrate (5.99 g) and iron(III) chloride hexahydrate (11.66 g) were separately dissolved in 100 mL of distilled water. The solutions were then combined in a beaker glass and stirred at 500 rpm using a magnetic stirrer at 50 °C. A 2 M NaOH solution was added dropwise to the precursor solution while stirring. The addition of NaOH was ceased when the pH reached 10. The resulting magnetite precipitate was separated by decantation, washed with distilled water, and precipitated again to remove excess water. Washing was repeated until the pH was neutral. The magnetite was filtered using Whatman 42 filter paper and dried in an oven at 100 °C until a constant mass of approximately 5 g was achieved.

Green Synthesis of Gaharu Leaf Extract-Modified Magnetite (MEDG)

Iron(II) sulfate heptahydrate (5.99 g) and iron(III) chloride hexahydrate (11.66 g) were dissolved in 75 mL of distilled water. The two solutions were mixed in a beaker glass and stirred at 500 rpm using a magnetic stirrer at 50 °C. Subsequently, 50 mL of gaharu leaf extract was added to the precursor solution and stirred for 10 min. A 2 M NaOH solution was then added dropwise while stirring continuously. The addition of NaOH solution was halted when the pH of the precursor reached 10. The resulting magnetite was washed with distilled water until the pH was neutral, filtered with Whatman 42 filter paper, and dried in an oven at 100 °C until a constant mass of approximately 5 g was achieved.

Characterization

The M and MEDG materials were characterized using several instruments: FTIR, PSA, SEM-EDX, XRD, and VSM. FTIR analysis was conducted using a PerkinElmer Spectrum IR 10.6.1 instrument with the KBr pellet method. Samples were mixed with KBr powders at a ratio of 1:10 (w:w) and pressed into transparent pellets. Particle size analysis (PSA) was performed using a Horiba SZ-100 (Z Type) Ver2.20 instrument. M and MEDG were dispersed in distilled water and sonicated for 30 min to aid dispersion. Although previous studies used sucrose solution as a dispersant for magnetite dispersion according to Horiba PSA (Klein, 1992), this study utilized pure distilled water as the dispersant. Surface morphology of M and MEDG was observed using a JEOL JED-2300 instrument at 20 kV. X-ray diffraction (XRD) analysis was conducted using a Rigaku Miniflex 600 Benchtop instrument, scanning samples from 10 to 80°. Vibrating sample magnetometer (VSM) analysis was performed using a VSM-250 instrument.

In addition to characterizing M and MEDG, their pH_{PZC} values were determined using the initial pH intercept method with a range of pH 2–10. A 0.05 M NaCl solution was adjusted to the desired pH using NaOH and HCl solutions. Ten miligrams of M, MEDG, and SDG were added to the NaCl solution, which was then allowed to stand for up to 2 × 24 h before measuring the final pH.

Methyl orange adsorption study

A total of 10 mL of 5 ppm methyl orange (MO) solution was adjusted to pH 2–10 by adding NaOH and HCl solutions. Then, 10 mg of adsorbent (M, MEDG, and SDG) was added to the solution and stirred using an orbital shaker at 150 rpm for 30 min. The optimum pH and contact time were determined by conducting adsorption at various pH levels (2–10) and contact times (10–90 min). Subsequently, adsorption at the optimum pH was conducted using MO concentrations ranging from 1–8 ppm. After adsorption, the MO solution was separated from M and MEDG using an external magnet, while SDG was separated by centrifugation. The absorbance of the MO solution was measured before and after adsorption using a UV–Vis spectrophotometer at a wavelength between 300 and 700 nm. The reusability of the adsorbent was also assessed by desorbing it with 1 M NaOH solution for 30 min, followed by drying at 100 ℃ for 15 min before reuse.

Result and discussion

Characterization

In this study, qualitative testing was conducted to detect the presence of flavonoid, tannin, and alkaloid compounds in gaharu leaf extract by adding specific reagents. The extract tested positive for flavonoids, indicated by a color change to reddish-orange, resulting from the reduction of flavonoids to flavonoid salts (Sankhalkar and Vernekar, 2016). Tannin presence was confirmed by a blackish-green solution formation, attributed to a complex compound between iron and tannin compounds (Sankhalkar and Vernekar, 2016). The orange color change during alkaloid compound analysis with Dragendorf's reagent indicated the presence of potassium quinoline compounds, formed from the reaction between alkaloid compounds and a complex compound of potassium tetraiodobismutat from Dragendorf's reagent (Raal et al., 2020). Consequently, gaharu leaf extract was qualitatively confirmed to contain flavonoids, tannins, and alkaloids.

Material characterization through FTIR analysis revealed distinctive peaks for M and MEDG (Fig. 1). M exhibited a sharp absorption peak at 547 cm^{-1}, attributed to tetrahedral and octahedral Fe—O stretching vibrations, while MEDG showed peaks at 590 and 693 cm^{-1} (Rasoulzadeh et al., 2019; Sebastian et al., 2019). Additionally, MEDG displayed an absorption peak at 425 cm^{-1}, corresponding to octahedral Fe—O bonds (Rasoulzadeh et al., 2019). Both M and MEDG exhibited absorption peaks at around 3350 cm^{-1}, indicative of O—H bonds (Altaf et al., 2021; Sulistyaningsih et al., 2017). The presence of C—H bonds was evident in both M and MEDG, with absorption peaks at 2925 and 2845 cm^{-1}, and in MEDG, peaks at 1462 and 912 cm^{-1} indicated the presence of C═C and C—C bonds, respectively (Loron et al., 2022; Rahmayanti et al., 2022). These bonds in MEDG are attributed to secondary metabolite compounds from gaharu leaf extract.

Referring to Fig. 1, the characteristics of MEDG compounds differ from those of M particles. MEDG exhibits additional bonds beyond Fe—O and O—H, originating from secondary metabolite compounds (flavonoid, tannin, and alkaloid). The O—H absorption peak intensity in MEDG is also higher than that in the M spectrum. This heightened intensity results from the presence of —OH groups in secondary metabolite compounds, enhancing the O—H vibrations in MEDG compared to M. Therefore, modifying magnetite using gaharu leaf extract increases the number of active groups on the particles (Fig. 2). Unlike M particles, which may have only one active group that can be protonated or deprotonated, MEDG particles possess numerous active sites. This modification with gaharu leaf extract provides additional active sites for

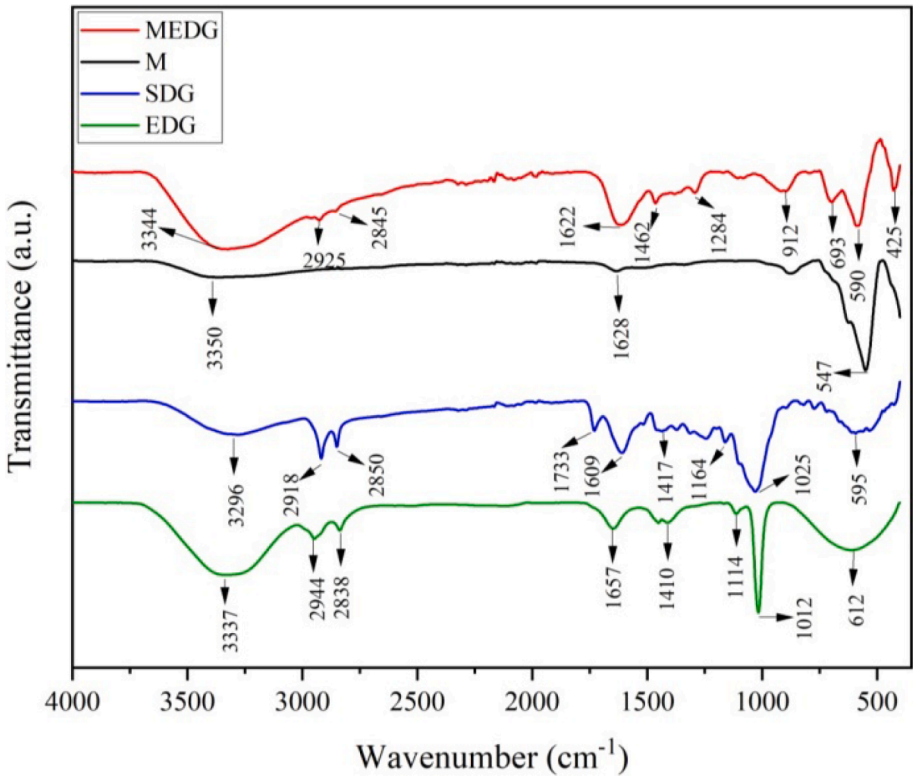

Fig. 1. IR spectra of M, MEDG, SDG, and EDG.

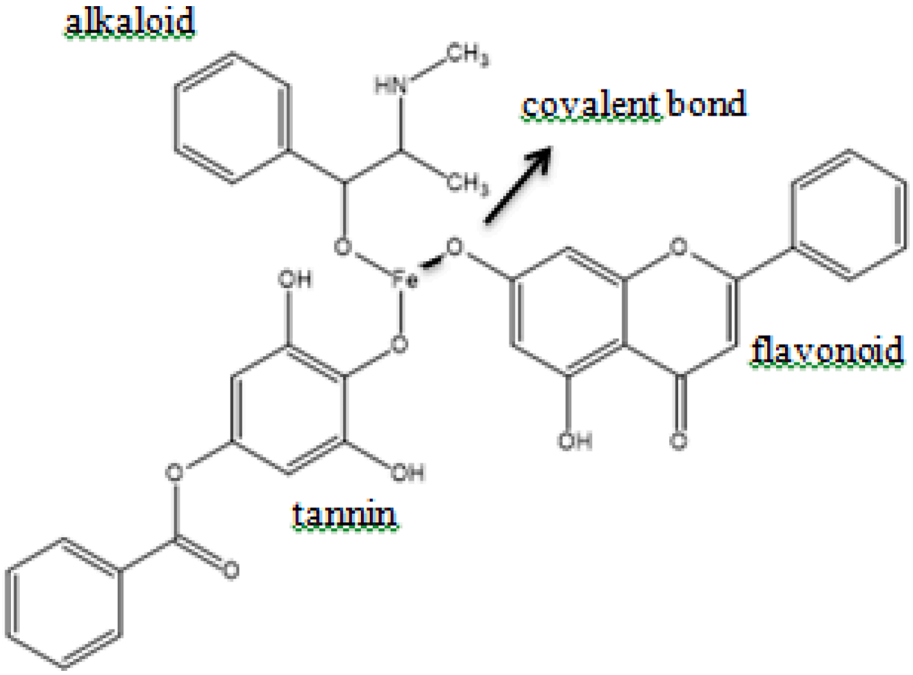

Fig. 2. Illustration of the bond between magnetite and secondary metabolite compounds.

binding the adsorbate, enhancing the adsorption ability of magnetite compared to unmodified magnetite.

Characterization of M and MEDG with PSA revealed that M particles were 4625 nm in size, whereas MEDG particles were smaller, specifically 4408.7 nm. The larger size of M particles is attributed to their tendency to aggregate during synthesis. In MEDG particles, the presence of

secondary metabolites inhibits this agglomeration process, resulting in smaller particle sizes. Coating magnetite surfaces with secondary metabolite compounds from gaharu leaf extract is expected to enhance the stability of magnetite in aqueous solutions. This increased stability reduces the agglomeration and settling of MEDG particles, resulting in smaller sizes than M particles. The stabilizing effect of secondary metabolite compounds from gaharu leaf extract on magnetite surfaces leads to smaller particle sizes, thereby increasing the surface area for enhanced adsorption capacity.

For effective particle size analysis, solid M and MEDG samples were dispersed in a disperser and sonicated to ensure single particle dispersion without agglomeration. In previous studies, sonication of particles before and after dispersion produced smaller magnetite particle sizes. The magnetite modification with jengkol bark extract showed that the particle sizes were 318 and 294 nm (Rahmayanti et al., 2022). The particles measuring 318 nm were obtained by modifying magnetite with 5 mL of jengkol bark extract for 0.5 g of magnetite, while the 294 nm particles were obtained by modifying with 15 mL of extract. In comparison, magnetite modified with Moringa oleifera leaf extract resulted in particle sizes of 50–60 nm (Altaf et al., 2021), with 25 mL of extract added for 1 g of magnetite. Similarly, magnetite modified with weed extract yielded particles measuring 250 nm, with 50 mL of concentrated extract added for 2 g of magnetite (Zulaicha et al., 2020). These studies suggest that the addition of more extract in magnetite synthesis leads to smaller particle sizes.

Additionally, sonication of magnetite particles before and after dispersion in a disperser can also influence particle size Altaf et al. (2021). Sonication is known to break down aggregates formed in magnetite, resulting in smaller particle sizes. Therefore, sonication can be used to control and reduce the size of magnetite particles during synthesis. However, in this study, sonication was performed only after dispersion for 30 min at a frequency of 40 kHz. This sonication aimed to break up any aggregates formed after magnetite dispersion in distilled water. Unlike previous studies, the M and MEDG particles in this study were not sonicated before dispersion, allowing them to form aggregates. Sonication after dispersion ensured that any aggregates formed were broken down, resulting in dispersed particles for accurate size analysis (Sulistyaningsih et al., 2013). However, the synthesized M and MEDG particles were not homogenized with a sieve, leading to microsized PSA results. This methodological difference explains the slight variation in particle size between M and MEDG.

The surface morphology of M and MEDG appeared spherical (Fig. 3). EDX analysis (Fig. 4) revealed that M contained a higher mass percentage of Fe atoms (94.41 %) compared to MEDG (60.18 %), whereas MEDG contained a higher mass percentage of O atoms (38.74 %) than M (2.18 %). The presence of secondary metabolite compounds from gaharu leaf extract in MEDG contributed to these differences. Functional groups containing oxygen atoms in the secondary metabolite compounds include hydroxyl (—OH), carbonyl (—CO—), and carboxyl groups (—COO—). MEDG showed a more homogeneous surface morphology with fewer aggregates compared to M particles (Basavaiah et al., 2018). This improved surface morphology of MEDG is attributed to secondary metabolite compounds binding to the magnetite surface, preventing the formation of aggregates. This happens because magnetite compounds at alkaline pH form Fe—O^- anions, which become nucleophilic and bind to secondary metabolite compounds, such as flavonoids, tannins, and alkaloids (Fig. 2). The coordination covalent bond between magnetite and secondary metabolite compounds enhances the magnetite surface, resulting in a more regular and homogeneous surface morphology in MEDG compared to M. The spherical surface morphology of MEDG contributes to its higher surface area, leading to increased adsorption capacity. Therefore, the modification of magnetite with gaharu leaf extract successfully enhanced its adsorption ability.

The particles of M exhibited a crystalline cubic shape, specifically face-centered cubic (fcc) (Rahmayanti et al., 2022), as confirmed by XRD results. In M particles, a diffractogram peak corresponds to the database COD 96-900-5839, while MEDG corresponds to database COD 96-900-2319 (Fig. 5). The crystal size of M particles was smaller, specifically 19.74 nm, whereas that of MEDG was 33.81 nm. The percentage crystallinity of M was 98.19 %, whereas that of MEDG was only 92.49 %. This reduction in crystallinity in MEDG is attributed to the presence of secondary metabolite compounds from gaharu leaf extract.

Characterization with VSM to determine the saturation magnetization of M and MEDG showed that the saturation magnetization of MEDG is smaller than that of M. The saturation magnetization value of M was 56.14 emu/g, while that of MEDG was only 34.43 emu/g (Fig. 6). This indicates that the addition of an extract of natural ingredients can reduce the saturation magnetization value of magnetite (Rahmayanti et al., 2022; Stan et al., 2019).

When magnetite is modified by adding gaharu leaf extract, the secondary metabolite compounds in the extract bond to the magnetite, coating the magnetite particles. This coating causes the crystallinity of magnetite to decrease because the organic compound is amorphous. The decrease in crystallinity is proportional to the binding of secondary metabolite compounds; the lower the crystallinity, the more secondary metabolite compounds are bound to magnetite.

Likewise, with saturation magnetization, the more secondary metabolite compounds are bound to magnetite, the lower the saturation

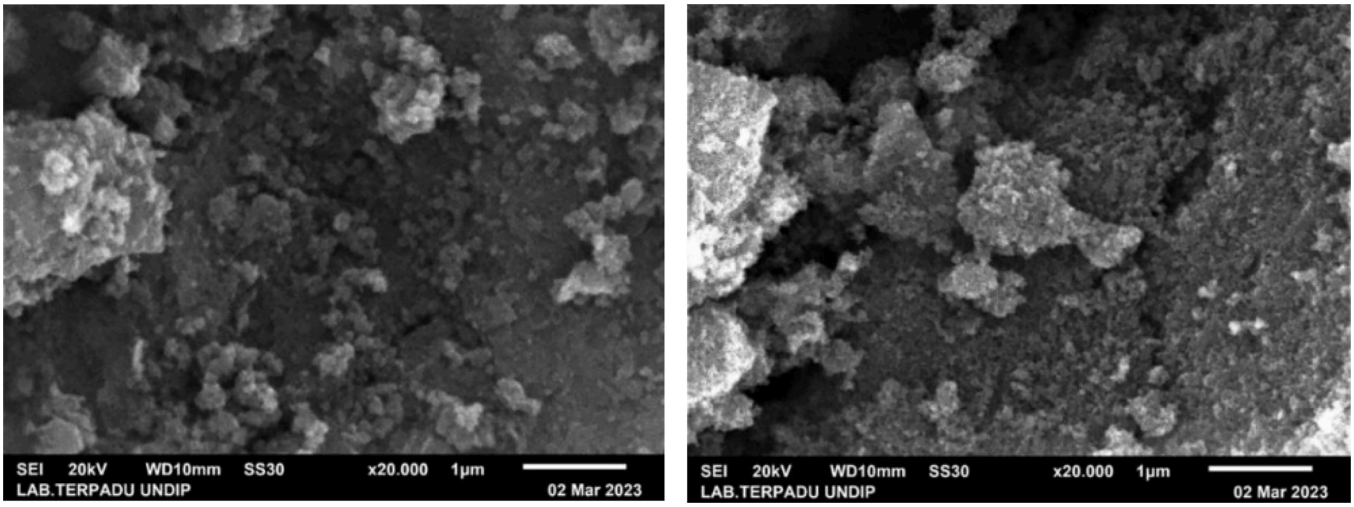

Fig. 3. Surface morphology of MEDG (left) and M (right).

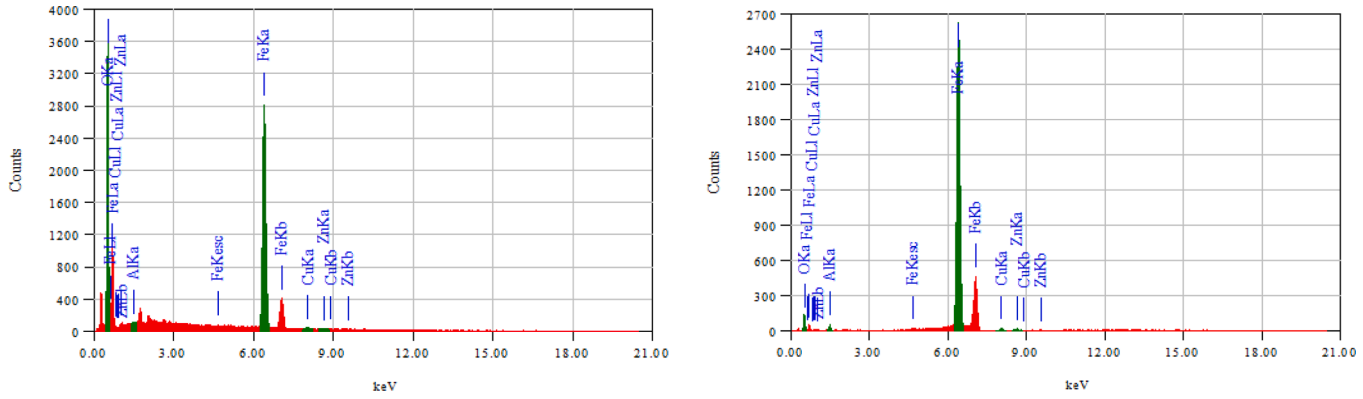

Fig. 4. EDX result of MEDG (left) and M (right).

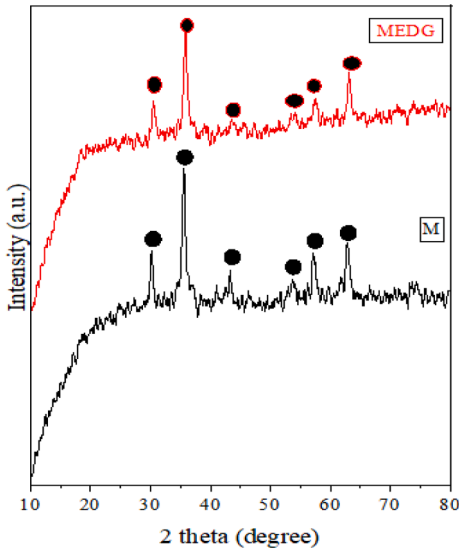

Fig. 5. Diffractogram of MEDG and M.

magnetization of magnetite. The addition of secondary metabolite compounds in magnetite increases the active sites in magnetite particles, thereby increasing their adsorption ability. Therefore, the decrease in crystallinity and saturation magnetization of MEDG compared to M aligns with the increase in MEDG adsorption ability.

Effect of pH, contact time, and adsorbate concentration on adsorption

The pH of a solution plays a crucial role in adsorption processes, as it determines the charge state of the adsorbent, whether it is protonated or deprotonated (Liberto et al., 2022). The point of zero charge (PZC) is the pH at which the surface of particles carries equal positive and negative charges (Kragović et al., 2019). Below the PZC, magnetite becomes positively charged ($Fe—OH_2^+$) and can adsorb anionic adsorbates effectively, while above the PZC, it becomes negatively charged ($Fe—O^-$) and can adsorb cationic adsorbates (Moirana et al., 2023). The pH_{PZC} values for M, MEDG, and SDG were determined to be 7.92, 7.61, and 5.97, respectively (Fig. 7). MEDG exhibited a lower pH_{PZC} than M, attributed to the presence of secondary metabolite compounds on its surface with carboxyl functional groups, making it more acidic (Altaf et al., 2021). This difference in pH_{PZC} also explains why SDG had an acidic pH_{PZC} value. Methyl orange, being an anionic compound, is best adsorbed in an acidic environment due to its negatively charged surface (Abate et al., 2021; Ahmad et al., 2022; Liberto et al., 2022).

The adsorption efficiency was determined by measuring the absorbance of the MO solution before and after adsorption at 464 nm using a UV–Vis spectrophotometer. The percentage of MO concentration adsorbed to the initial concentration was then calculated. The adsorption of MO onto MEDG and SDG was most efficient at pH 3, while M was most efficient at pH 4 (Fig. 8). The color of the MO solution changed from red at pH 3 to orange at pH 4, indicating successful adsorption by the adsorbents (M, MEDG, and SDG). MEDG exhibited the highest adsorption efficiency at 95.62 %, followed by SDG at 77.95 %, and M at 74.76 %. This improvement in adsorption ability can be attributed to the organic functional groups on the MEDG surface, enhancing its interaction with MO. The successful modification of magnetite with gaharu leaf extract to increase its adsorption ability was thus achieved. MEDG's higher adsorption efficiency compared to M can be attributed to its greater number of active sites, stemming from the secondary metabolite compounds in the gaharu leaf extract. Additionally, MEDG's superior size and morphology contributed to its higher surface area, further enhancing its adsorption capacity.

In this study, the influence of contact time and adsorbate concentration on the adsorption process was investigated alongside pH optimization. The adsorption time during pH optimization was set at 30 min using an MO concentration of 5 ppm. Following the determination of the optimum pH, adsorption experiments were conducted at this pH with varying contact times ranging from 10 to 90 min. Contact time is a critical factor as it indicates the duration required for maximum adsorbate (MO) uptake. Beyond the optimal contact time, adsorbents become saturated, limiting their adsorption capacity. Thus, the objective was to determine the optimal contact time for adsorbing an MO solution at concentrations of 5 ppm and pH levels of 3–4. The results revealed that the optimal contact time for MO adsorption by MEDG and SDG adsorbents was 60 min, while for M, it was 70 min (Fig. 9). MEDG and SDG exhibited faster adsorption rates due to their higher number of active sites, which are essential for MO adsorption and are provided by the secondary metabolite compounds present in gaharu leaves.

Under optimal pH and contact time conditions, adsorption experiments were conducted using varying concentrations of the MO solution to determine the optimal concentration for adsorption using the adsorbents (M, MEDG, and SDG). The initial concentration of the MO solution used during pH and contact time optimization was 5 ppm. The results indicated that the optimal concentration of the MO solution for adsorption was 5 ppm (Fig. 10). Thus, under the optimum conditions (pH 3 for 60 min for MEDG and SDG, and pH 4 for 70 min for M), the

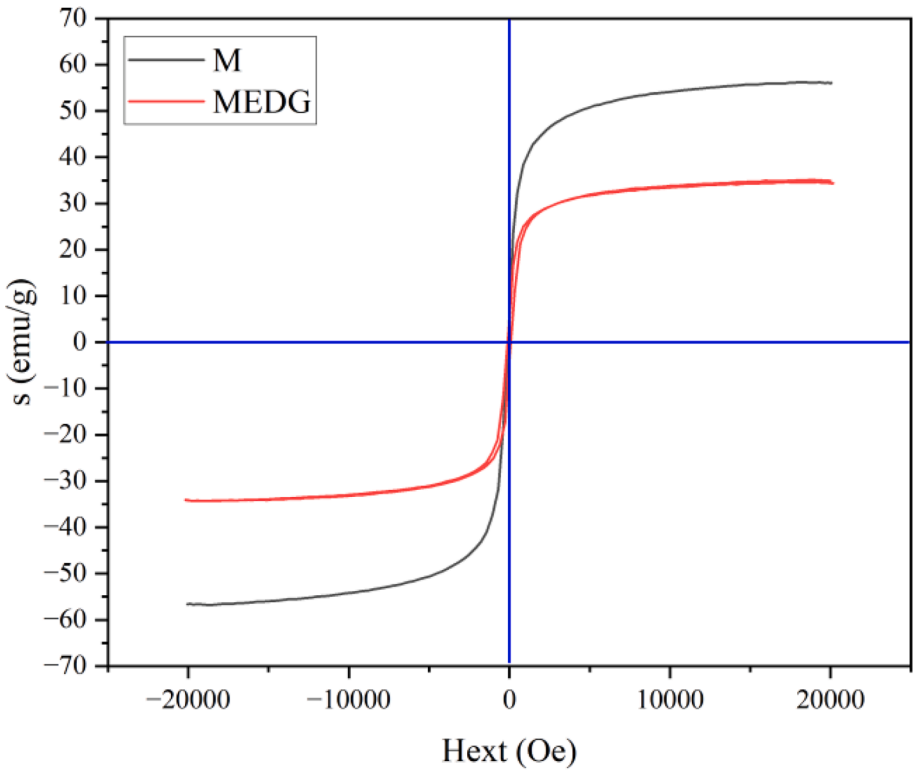

Fig. 6. Magnetization curve of MEDG and M.

adsorption capacity becomes saturated. Adsorption below the optimal concentration occurs easily, while above the optimal concentration, the adsorbents reach their maximum adsorption capacity, illustrating the concept of optimum concentration.

MO compounds are anionic in aqueous solutions, and they are maximally absorbed by adsorbents with cationic surfaces. Magnetite becomes cationic when the pH of the adsorbate solution is below its point of zero charge (pH_{PZC}). Since the pH_{PZC} of both M and MEDG ranges between 7 and 8, the optimal pH for MO compound adsorption is acidic. This study determined the optimum pH for MO compound adsorption to be pH 3 for MEDG and pH 4 for M, based on theoretical considerations and previous research. At acidic pH, the surface of magnetite (M) becomes positively charged ($Fe—OH_2^+$), enabling the anionic MO compound to bind to the magnetite surface. The bonds formed are ionic (Fig. 11). In contrast, the bond between MEDG and MO is a coordination covalent bond, formed through nucleophilic substitution reactions (Fig 12). In this reaction, MO acts as an anion and plays a nucleophilic role, attacking the substrate compound (MEDG) to form a new bond through a coordination covalent bond.

MEDG exhibits more active sites than M, resulting in higher adsorption ability, as confirmed by PSA and SEM results indicating superior size and surface morphology. Consequently, the optimum adsorption time for MEDG is shorter than for M. Despite SDG's higher content of secondary metabolite compounds compared to MEDG, the study found that both SDG and MEDG have an optimum adsorption time of 60 min. This unexpected finding is attributed to the lightweight nature of SDG, which causes it to float on the surface of the MO solution during adsorption, reducing its contact area with the MO compound despite having many active sites. In conclusion, modifying magnetite with gaharu leaf extract enhances its adsorption ability compared to M and SDG, as demonstrated by the results of this study.

Adsorption kinetics

Adsorption kinetics were investigated by varying the contact time from 10 to 90 min. Maximum adsorption for M was observed at 70 min, while for MEDG and SDG it was at 60 min, indicating faster adsorption with MEDG and SDG due to the presence of organic compounds. The adsorption kinetics were modeled using Lagergren's pseudo-first-order and Ho's pseudo-second-order models (Tables 1 and 2). Lagergren's pseudo-first-order model is described by equation (1), where the graph of log(qe–qt) against time (t) represents the adsorption process. Ho's pseudo-second-order model is described by equation (2), with the graph of t/qt against time (t) depicting the adsorption.

The adsorption kinetics model graphs (Fig. 13) indicated that the adsorption of MO by M, MEDG, and SDG followed Ho's pseudo-second-order model, as evidenced by the correlation coefficient (R2) values. The R2 values for Lagergren's pseudo-first-order model for M, MEDG, and SDG were 0.7855, 0.9597, and 0.8382, respectively, smaller than the corresponding values for Ho's pseudo-second-order model, which were 0.9532, 0.9973, and 0.9498. This indicates that the adsorption capacity of MO was proportional to the number of active sites of the adsorbent used, and the adsorption occurred through chemisorption.

$$\log(qe - qt) = \log qe - \frac{k}{2.303}t \quad (1)$$

$$\frac{t}{qt} = \frac{t}{qe} + \frac{1}{k.qe^2} \quad (2)$$

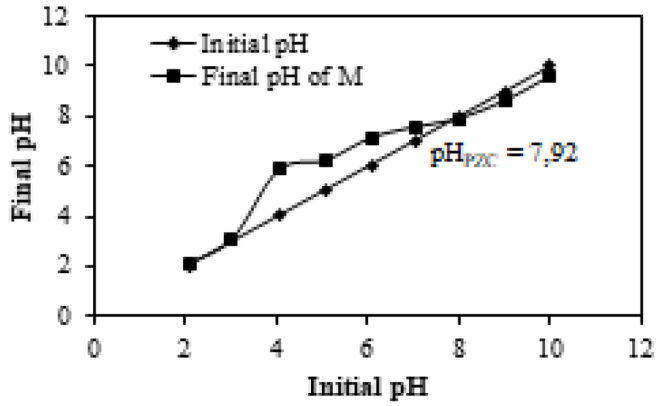

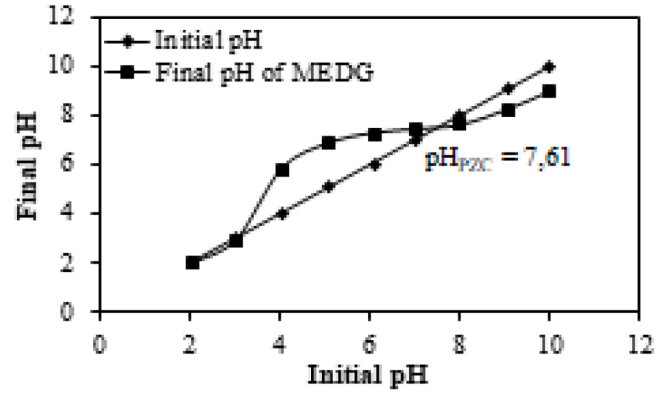

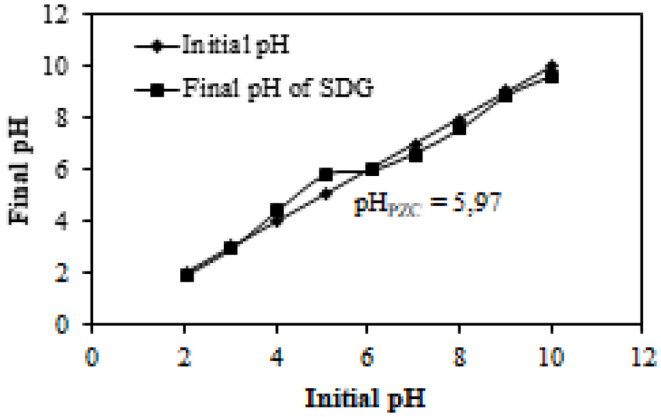

Fig. 7. pH_{PZC} of M, MEDG, and SDG.

Adsorption isotherm

The adsorption isotherm in this study was investigated using variations in the concentration of the MO solution and modeled using Langmuir and Freundlich's isotherm models (Table 3 and 4). Langmuir's isotherm model suggests that adsorption occurs in a monolayer on the adsorbent's surface with uniform energy distribution across all active sites (Rahmayanti et al., 2022). The Langmuir equation is represented by equation (3), where Ce is the concentration of the solution (mg/L) and qe is the adsorption capacity (mg/g), plotted as Ce/qe against Ce. On the other hand, Freundlich's model indicates multilayer adsorption with heterogeneous energy distribution. Equation (4) describes the Freundlich model, with the graph plotted as log qe (y-axis) against log Ce (x-axis).

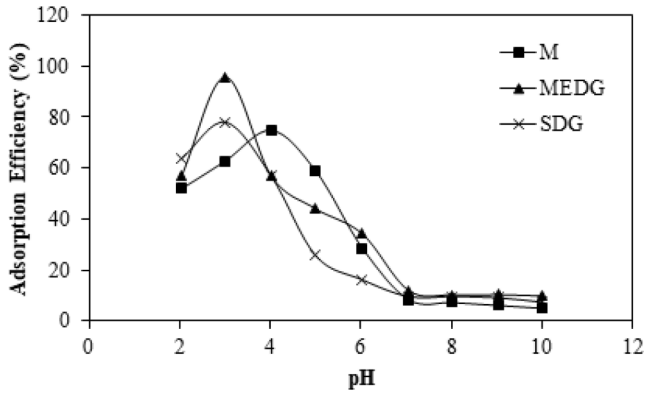

Fig. 8. Determination of adsorption optimum pH point.

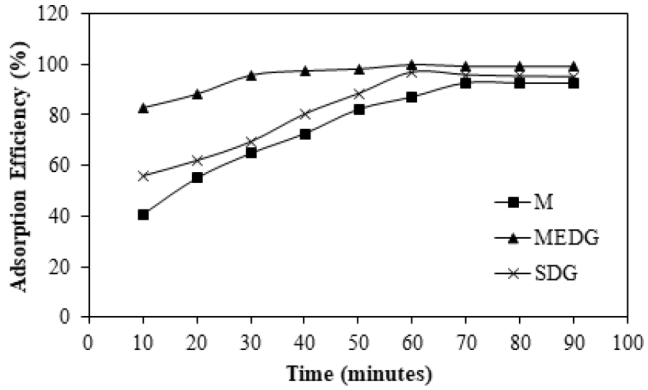

Fig. 9. Determination of the optimum contact time for adsorption.

The results showed that MO adsorption followed Freundlich's isotherm model, with R^2 values of 0.9425, 0.9477, and 0.9475 for M, MEDG, and SDG adsorbents, respectively (Fig. 14). In contrast, the R^2 values for Langmuir's isotherm model were lower at 0.7259, 0.7285, and 0.7283, respectively. The Freundlich isotherm model is suitable for describing physical adsorption on heterogeneous surfaces in multiple layers, where adsorption occurs with weaker bonds. The isotherm constant (KF) value indicates the adsorption capacity qualitatively, with higher values indicating greater capacity. The MEDG adsorbent exhibited the highest KF value, suggesting the highest adsorption capacity among the three adsorbents.

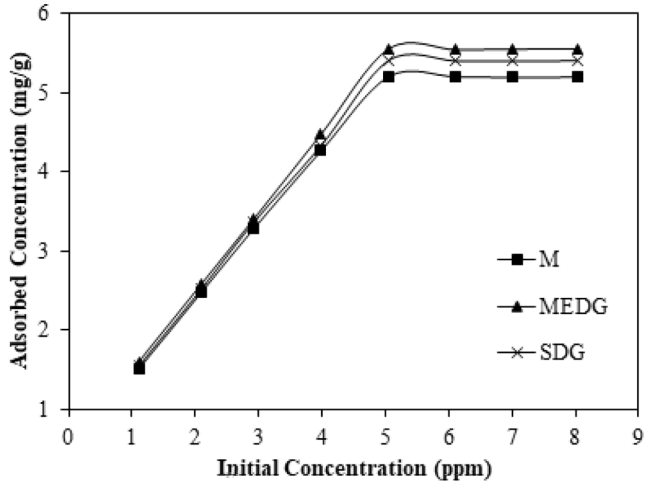

Fig. 10. Determination of the optimum adsorbate concentration for adsorption.

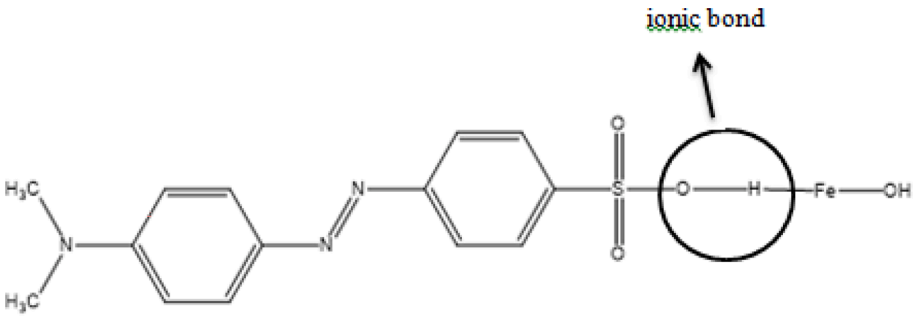

Fig. 11. The bond between M compound and MO.

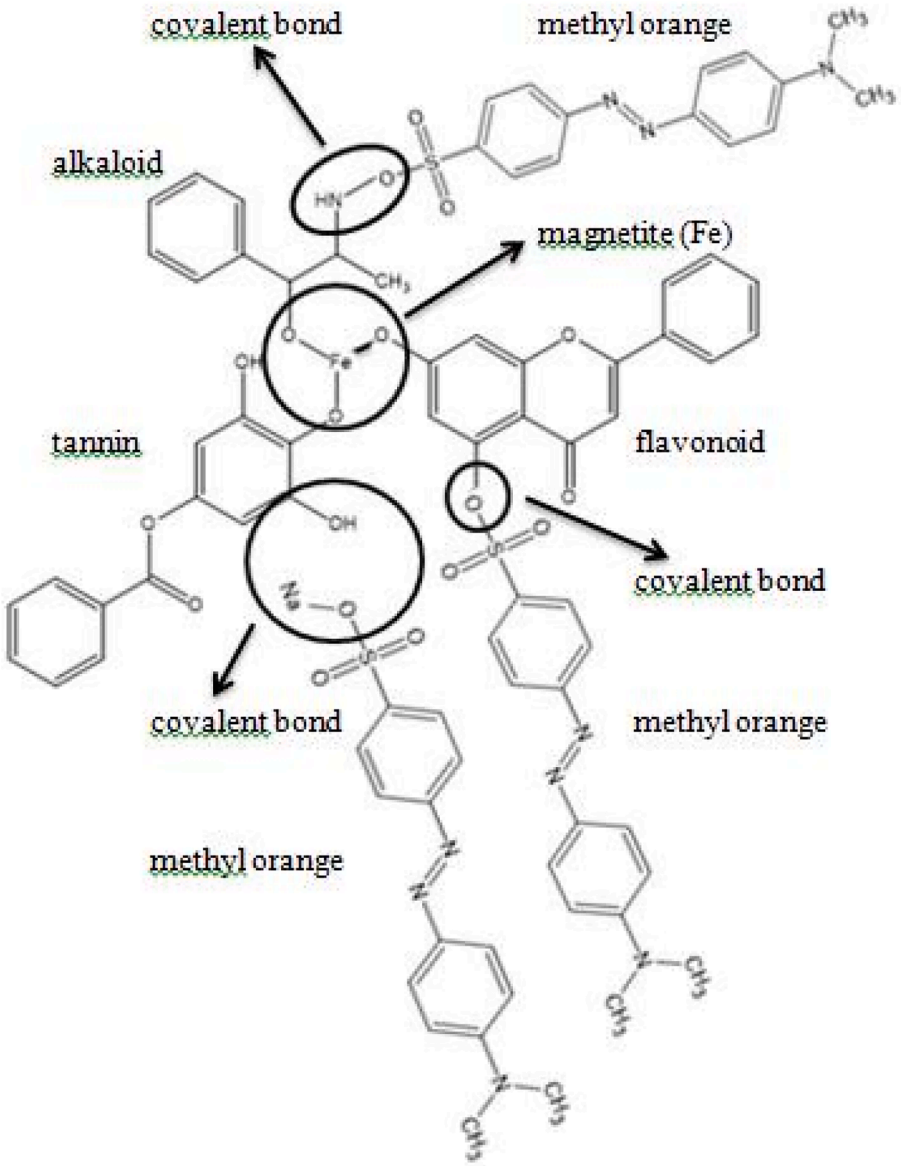

Fig. 12. The bond between MEDG compound and MO.

Additionally, the adsorption kinetics results showed that the adsorption rate followed a pseudo-second-order model. This indicates that the adsorption rate is directly proportional to the decrease in MO concentration over time until equilibrium is reached. The MEDG adsorbent absorbed MO rapidly from the beginning, leading to a less significant increase in adsorption rate. The adsorption kinetics results, along with the optimum adsorption conditions, support the conclusion that the adsorption kinetics followed the pseudo-second-order model and Freundlich's model.

$$\frac{Ce}{qe} = \frac{Ce}{q_{max}} + \frac{1}{q_{max}.K_L} \quad (3)$$

Table 1
Calculated values of parameters in Lagergren's pseudo-first-order equation.

Adsorbent	R^2	qe (mg/g)	k (min^{-1})
M	0.7855	7.0046	0.0534
MEDG	0.9749	3.3658	0.0803
SDG	0.8382	4.5535	0.0478

Table 2
Calculated values of parameters in Ho's pseudo-second-order equation.

Adsorbent	R^2	qe (mg/g)	k (g/mg·min)
M	0.9772	6.4153	0.0058
MEDG	0.9990	5.5163	0.0301
SDG	0.9842	5.6120	0.0124

$$\log qe = \frac{1}{n}\log Ce + \log K_F \quad (4)$$

Reusability

The reusability of an adsorbent refers to its ability to be reused after adsorption. In this study, the reusability of the adsorbent was investigated under optimum adsorption conditions, including pH, contact time, and adsorbate concentration. After each adsorption cycle, the adsorbent was desorbed to remove the MO compound.

The results showed that M and MEDG could be reused up to 5 times, while SDG was only reusable for 3 times. The adsorption ability of M and MEDG remained high, around 95–99 %, for the first 4 repetitions, but decreased to 87 % for the fifth repetition. For SDG, the adsorption ability was 98.18 and 95.21 % for the first and second repetitions, respectively,

Table 3
Calculated values of parameters in Langmuir's equation.

Adsorbent	R^2	q_{max} (mol/g)	K_L (L/mol)
M	0.7259	11.6777	0.1095
MEDG	0.7285	12.4304	0.1010
SDG	0.7283	12.3186	0.1013

Table 4
Calculated values of parameters in Freundlich's equation.

Adsorbent	R^2	n	K_F(mol/g)
M	0.9425	1.2424	1.1279
MEDG	0.9477	1.2419	1.1359
SDG	0.9475	1.2425	1.1286

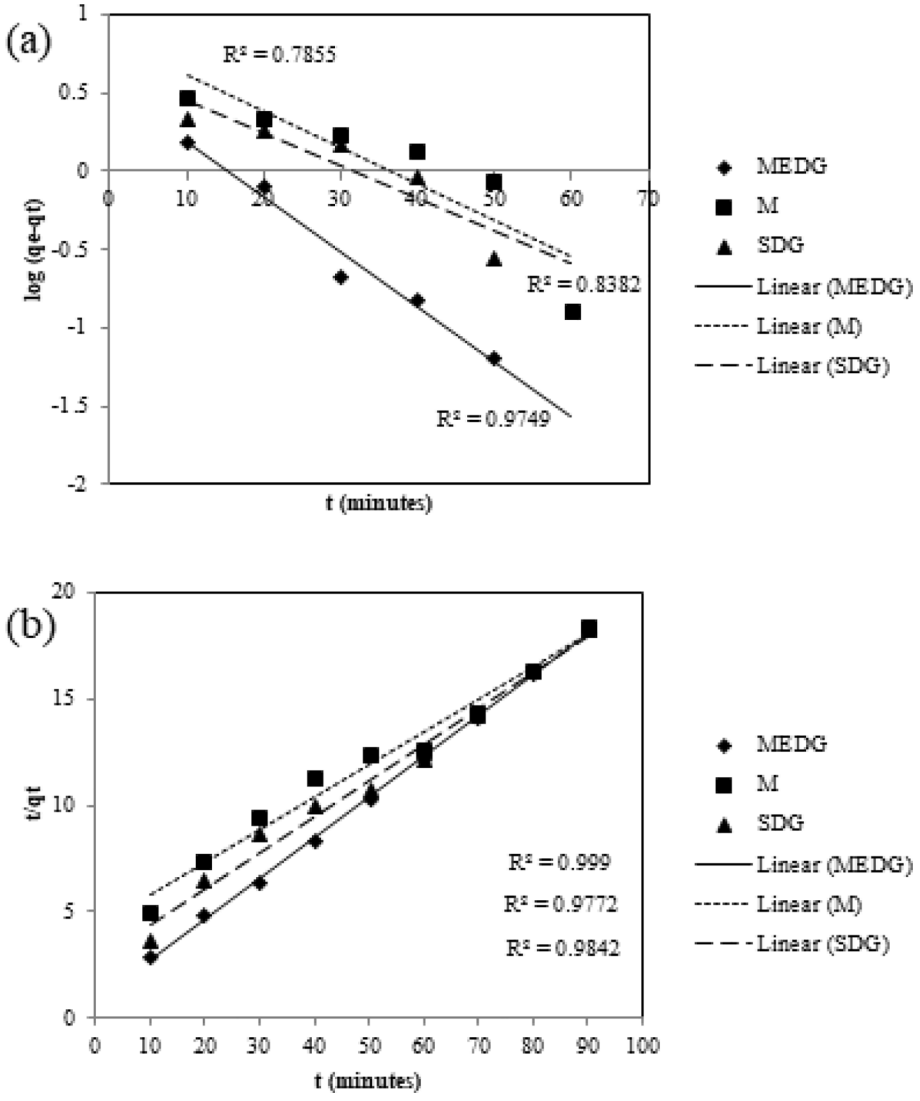

Fig. 13. (a) Lagergren's pseudo-first-order and (b) Ho's pseudo-second-order adsorption kinetic plots.

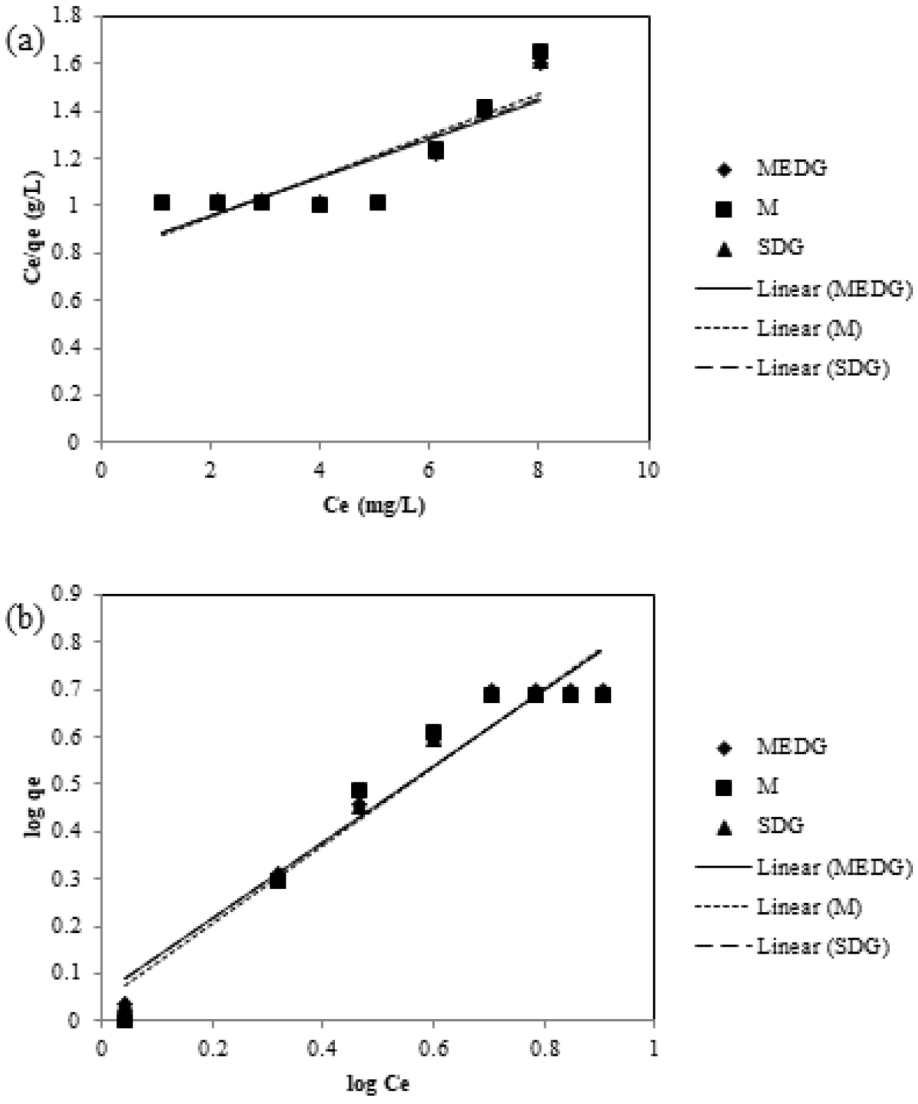

Fig. 14. (a) Langmuir and (b) Freundlich adsorption isotherm plots.

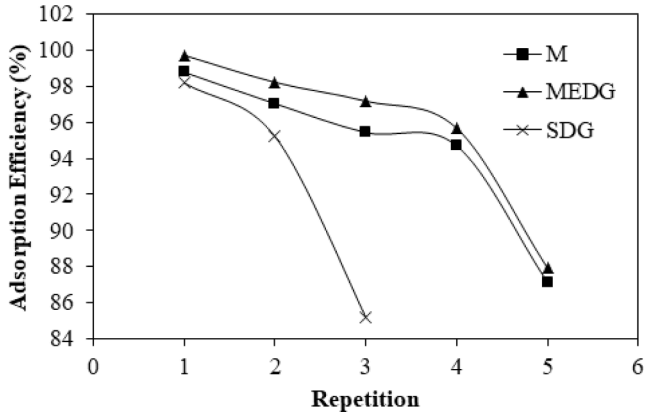

Fig. 15. Adsorption efficiency of adsorbent after reusable.

but decreased to 85.19 % for the third repetition (Fig. 15).

In the SDG adsorbent, the adsorption efficiency decreased rapidly and significantly, especially in the third repetition. This is attributed to SDG's lightweight characteristics, which make it slow to settle. During desorption, the adsorbent is separated from the adsorbate solution, and

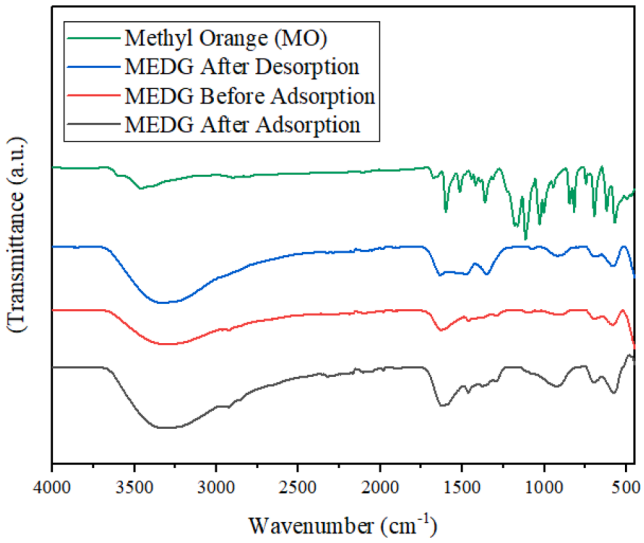

Fig. 16. IR spectra of MEDG after and before adsorption in the reusable stage.

the MO compound bound to the adsorbent is released and collected in the desorption medium. M and MEDG are separated from the adsorbate using an external magnet, minimizing wastage during decantation. In contrast, SDG needs to be centrifuged to settle, leading to some SDG particles remaining suspended and being wasted during decantation. This causes a decrease in the mass of the SDG adsorbent, leading to reduced adsorption efficiency in subsequent repetitions. Therefore, SDG is less economical to use as an adsorbent due to its lightweight nature and difficulty in settling.

After adsorption and desorption, the adsorbent was characterized using FTIR. The adsorbent that had bound the MO compound exhibited sharper peaks at wavenumbers ranging from 750 to 1750 cm^{-1} compared to the adsorbent before adsorption (Fig. 16). MEDG and SDG showed absorption peaks in this range. The sharpness of the peaks increased after adsorption, indicating the formation of bonds between the adsorbent and MO compound. The MO compound, being an organic compound, has organic bonds in this wavenumber range, leading to increased intensity of the absorption peaks. After desorption, the peak sharpness at these wavenumbers decreased, and the spectra were almost identical to those before adsorption. The N═N bond of MO is typically observed at absorption peaks in the wavenumber region of 1500–1600 cm^{-1} (Cyril et al., 2019).

Conclusion

Based on the research findings, magnetite (M) and gaharu leaf extract-modified magnetite (MEDG) were successfully synthesized using the coprecipitation method. The infrared (IR) spectra revealed that MEDG exhibited more absorption peaks than M, indicating a higher number of active sites due to the presence of secondary metabolite compounds from gaharu leaf extract. While both particles displayed spherical morphology, MEDG particles were more uniform in shape compared to M. Additionally, MEDG had smaller particle size and higher oxygen atom content.

M particles exhibited face-centered cubic crystals with higher crystallinity than MEDG. The addition of gaharu leaf extract led to a decrease in the saturation magnetization value of magnetite. This modification increased the number of active sites on the particles and reduced particle size, preventing aggregation in aqueous solutions. Furthermore, the surface morphology of modified magnetite became more regular compared to pure magnetite. Although this modification reduced particle crystallinity and saturation magnetization, the increased number of active sites enhanced the adsorption ability of the particles.

The optimum pH for adsorption of methyl orange (MO) with MEDG, SDG, and M as adsorbents was found to be pH 3, 3, and 4, respectively. The optimal contact time was determined to be 60, 60, and 70 min, while the optimum MO concentration was 5 ppm. Adsorption kinetics followed Ho's pseudo-second order model, indicating a multilayer interaction, while the adsorption isotherm followed Freundlich's model.

Furthermore, the modification of magnetite with gaharu leaf extract significantly increased its adsorption ability, with MEDG achieving an adsorption efficiency of 95 %. Moreover, MEDG could be reused up to 5 times. Therefore, the modification of magnetite with gaharu leaf extract is recommended as an effective adsorbent for removing MO textile dyes.

CRediT authorship contribution statement

Triastuti Sulistyaningsih: Writing – review & editing, Validation, Data curation, Conceptualization. **Dwi Atika Sari:** Writing – original draft, Investigation, Methodology, Visualization. **Nuni Widiarti:** Validation, Methodology. **Widi Astuti:** Validation, Conceptualization. **Rika Wulandari:** Writing – review & editing, Validation, Conceptualization. **Dewanto Harjunowibowo:** Validation, Writing – review & editing.

Declaration of competing interest

The authors declare that they have no known competing financial interests or personal relationships that could have appeared to influence the work reported in this paper.

Acknowledgments

The authors gratefully acknowledge Universitas Negeri Semarang Indonesia for providing financial support through a basic research grant (contact number SP DPA 023.17.2.690645/2023.10). The authors also extend their gratitude to the Chemistry Department's Laboratory of Universitas Negeri Semarang for their support and facilities during this research. Additionally, the authors acknowledge the Integrated Laboratory of Universitas Diponegoro and Universitas Negeri Yogyakarta for their support in characterization. Special thanks are also due to the Advanced Characterization Laboratories Serpong, National Research and Innovation Agency through E-Layanan Sains, Badan Riset dan Inovasi Nasional (BRIN), for their facilities, scientific, and technical support.

References

Abate, G.Y., Alene, A.N., Habte, A.T., Addis, Y.A., 2021. Adsorptive removal of basic green dye from aqueous solution using humic acid modified magnetite nanoparticles: kinetics, equilibrium and thermodynamic studies. J. Polym. Environ. 29 (3), 967–984. https://doi.org/10.1007/s10924-020-01932-3.

Ahmad, A., Al-Swaidan, H.M., Alghamdi, A.H., Alotaibi, K.M., Hatshan, M.R., Haider, S., Khan, I., 2024. Facile synthesis of mesoporous active carbon from the valorisation of biomass waste and assessment of sequester efficiency of arsenic (As) from water. J. Anal. Appl. Pyrol. 177, 106304 https://doi.org/10.1016/j.jaap.2023.106304.

Ahmad, N., Suryani Arsyad, F., Royani, I., Lesbani, A., 2022. Adsorption of methylene blue on magnetite humic acid: kinetic, isotherm, thermodynamic, and regeneration studies. Res. Chem. 4, 100629 https://doi.org/10.1016/j.rechem.2022.100629.

Al-husseiny, R.A., Ebrahim, S.E., 2022. Synthesis of nano-magnetite and magnetite/synthetic geopolymer nano-porous composite for application as a novel adsorbent. Environ. Nanotechnol. Monit. Manage. 18, 100700 https://doi.org/10.1016/J.ENMM.2022.100700.

Altaf, S., Zafar, R., Zaman, W.Q., Ahmad, S., Yaqoob, K., Syed, A., Khan, A.J., Bilal, M., Arshad, M., 2021. Removal of levofloxacin from aqueous solution by green synthesized magnetite (Fe_3O_4) nanoparticles using Moringa olifera: kinetics and reaction mechanism analysis. Ecotoxicol. Environ. Saf. 226, 1–11. https://doi.org/10.1016/j.ecoenv.2021.112826.

Astuti, W., Sulistyaningsih, T., Maksiola, M., 2017. Equilibrium and kinetics of adsorption of methyl violet from aqueous solutions using modified *Ceiba pentandra sawdust*. Asian J. Chem. 29 (1), 133–138. https://doi.org/10.14233/ajchem.2017.20158.

Astuti, Widi, Sulistyaningsih, T., Prastiyanto, D., Purba, B.S.A., Kusumawardani, R., 2020. Synthesis of magnetically separable activated carbon from pineapple crown leaf for zinc ion removal. Mater. Sci. Forum 1007 (1), 71–75. https://doi.org/10.4028/www.scientific.net/MSF.1007.71.

Astuti, W., Sulistyaningsih, T., Prastiyanto, D., Rusiyanto, L., Riayanti, F.I., Astuti, A.W., Wibowo, W.T., Handayani, A.D., Wulandari, D.A., 2023. Influence of lignocellulosic composition in biomass waste on the microstructure and dye adsorption characteristics of microwave-assisted $ZnCl_2$ activated carbon. Biomass Convers. Biorefin. https://doi.org/10.1007/s13399-023-04281-y, 0123456789.

Basavaiah, K., Kahsay, M.H., RamaDevi, D., 2018. Green synthesis of magnetite nanoparticles using aqueous pod extract of *Dolichos lablab* L for an efficient adsorption of crystal violet. Emerg. Mater. 1, 121–132. https://doi.org/10.1007/s42247-018-0005-1.

Cai, W., Weng, X., Chen, Z., 2019. Highly efficient removal of antibiotic rifampicin from aqueous solution using green synthesis of recyclable nano- Fe_3O_4. Environ. Pollut. 247, 839–846. https://doi.org/10.1016/j.envpol.2019.01.108.

Cyril, N., George, J.B., Joseph, L., Sylas, V.P., 2019. Catalytic degradation of methyl Orange and selective sensing of mercury ion in aqueous solutions using green synthesized silver nanoparticles from the seeds of *Derris trifoliata*. J. Clust. Sci. 30 (2), 459–468. https://doi.org/10.1007/s10876-019-01508-9.

Da Gama, S.K.J., Saputri, R., Hidayati, R., 2021. Comparison method of extraction to Total flavonoid convention of 70% ethanol extract of gaharu leaves (Aquilaria microcarpa Baill). Jurnal Jamu Kusuma 1 (2), 51–56. https://doi.org/10.37341/jurnaljamukusuma.v1i2.11.

Das, A.K., Marwal, A., Verma, R., 2014. Datura inoxia leaf extract mediated one step green synthesis and characterization of magnetite (Fe_3O_4) nanoparticles. J. Pharm. Nanotechnol. 2 (2), 21–24.

Dash, A., Ahmed, M.T., Selvaraj, R., 2019. Mesoporous magnetite nanoparticles synthesis using the *Peltophorum pterocarpum* pod extract, their antibacterial efficacy against pathogens and ability to remove a pollutant dye. J. Mol. Struct. 1178, 268–273. https://doi.org/10.1016/j.molstruc.2018.10.042.

De Oliveira, L.H., Pereira, M.V., Meneguin, J.G., De Barros, M.A.S.D., Do Nascimento, J. F., Arroyo, P.A., 2023. Influence of regeneration conditions on cyclic CO_2 adsorption on NaA zeolite at high pressures. J. CO2 Util. 67 (April 2022) https://doi.org/10.1016/j.jcou.2022.102296.

El-kammah, M., Elkhatib, E., Gouveia, S., Cameselle, C., Aboukila, E., 2022. Cost-effective ecofriendly nanoparticles for rapid and efficient indigo carmine dye removal from wastewater: adsorption equilibrium, kinetics and mechanism. Environ. Technol. Innov. 28, 1–10. https://doi.org/10.1016/j.eti.2022.102595.

Hashmi, S.S., Shah, M., Muhammad, W., Ahmad, A., Ullah, M.A., Nadeem, M., Abbasi, B. H., 2021. Potentials of phyto-fabricated nanoparticles as ecofriendly agents for photocatalytic degradation of toxic dyes and waste water treatment, risk assessment and probable mechanism. J. Indian Chem. Soc. 98 (4), 100019 https://doi.org/10.1016/j.jics.2021.100019.

Huda, N., Muin, A., Fahrizal., 2015. Asosiasi fungi mikoriza arbuskula (FMA) pada tanaman gaharu aquilaria spp di desa laman satong kabupaten ketapang. Jurnal Hutan Lestari 4 (1), 72–81.

Hussain, S., Kamran, M., Khan, S.A., Shaheen, K., Shah, Z., Suo, H., Khan, Q., Shah, A.B., Rehman, W.U., Al-Ghamdi, Y.O., Ghani, U., 2021. Adsorption, kinetics and thermodynamics studies of methyl orange dye sequestration through chitosan composites films. Int. J. Biol. Macromol. 168, 383–394. https://doi.org/10.1016/j.ijbiomac.2020.12.054.

Iwuozor, K.O., Ighalo, J.O., Emenike, E.C., Ogunfowora, L.A., Igwegbe, C.A., 2021. Adsorption of methyl orange: a review on adsorbent performance. Curr. Res. Green Sustain. Chem. 4 (July) https://doi.org/10.1016/j.crgsc.2021.100179.

Klein, B., 1992. Rheology and Stability of Magnetite Dense Media (Issue May). The University of British Columbia Vancouver, Canada.

Kosheleva, R.I., Mitropoulos, A.C., Kyzas, G.Z., 2019. Synthesis of activated carbon from food waste. Environ. Chem. Lett. 17 (1), 429–438. https://doi.org/10.1007/s10311-018-0817-5.

Kragović, M., Stojmenović, M., Petrović, J., Loredo, J., Pašalić, S., Nedeljković, A., Ristović, I., 2019. Influence of alginate encapsulation on point of zero charge (pHpzc) and thermodynamic properties of the natural and Fe(III)-modified zeolite. Procedia Manuf. 32, 286–293. https://doi.org/10.1016/j.promfg.2019.02.216.

Liberto, G.D., Maleki, F., Pacchioni, G., 2022. PH dependence of MgO, TiO_2, and γ-Al_2O_3 surface chemistry from first principles. J. Phys. Chem. C 126 (24), 10216–10223. https://doi.org/10.1021/acs.jpcc.2c02289.

Lohrasbi, S., Kouhbanani, M.A.J., Beheshtkhoo, N., Ghasemi, Y., Amani, A.M., Taghizadeh, S., 2019. Green synthesis of iron nanoparticles using *Plantago major* leaf extract and their application as a catalyst for the decolorization of azo dye. BioNanoScience 9 (2), 317–322. https://doi.org/10.1007/s12668-019-0596-x.

López, Y.C., Antuch, M., 2020. Morphology control in the plant-mediated synthesis of magnetite nanoparticles. Green Sustain. Chem. https://doi.org/10.1016/j.cogsc.2020.02.001.

Loron, C.C., Sforna, M.C., Borondics, F., Sandt, C., Javaux, E.J., 2022. Synchrotron FTIR investigations of kerogen from proterozoic organic-walled eukaryotic microfossils. Vib. Spectrosc 123 (November). https://doi.org/10.1016/j.vibspec.2022.103476.

Maheswari, K.C., Reddy, P.S., 2016. Green synthesis of magnetite nanoparticles through leaf extract of *Azadirachta indica*. J. Nanosci. Technol. 2 (4), 189–191.

Masalvad, S.K.S., Sakare, P.K., 2020. Application of photo Fenton process for treatment of textile Congo-red dye solution. Mater. Today: Proc. 46, 5291–5297. https://doi.org/10.1016/j.matpr.2020.08.650.

Masuku, M., Ouma, L., Pholosi, A., 2021. Microwave assisted synthesis of oleic acid modified magnetite nanoparticles for benzene adsorption. Environ. Nanotechnol. Monit. Manage. 15 (September 2020) https://doi.org/10.1016/j.enmm.2021.100429.

Mittal, A.K., Chisti, Y., Banerjee, U.C., 2013. Synthesis of metallic nanoparticles using plant extracts. Biotechnol. Adv. 31 (2), 346–356. https://doi.org/10.1016/j.biotechadv.2013.01.003.

Mohammadzadeh, M., Leiviskä, T., 2023. Iron-modified peat and magnetite-pine bark biosorbents for levofloxacin and trimethoprim removal from synthetic water and various pharmaceuticals from real wastewater. Ind. Crop. Prod. 195 (December 2022) https://doi.org/10.1016/j.indcrop.2023.116491.

Moirana, R.L., Mkunda, J., Machunda, R., Paradelo, M., Mtei, K., 2023. Hydroxyapatite-activated seaweed biochar for enhanced remediation of fluoride contaminated soil at various pH ranges. Environ. Adv. 11, 100329 https://doi.org/10.1016/j.envadv.2022.100329.

Oyetade, J.A., Machunda, R.L., Hilonga, A., 2022. Photocatalytic degradation of azo dyes in textile wastewater by polyaniline composite catalyst-a review. Sci. Afr. 17, e01305.

Padhi, D.K., Panigrahi, T.K., Parida, K., Singh, S.K., Mishra, P.M., 2017. Green synthesis of Fe_3O_4/RGO nanocomposite with enhanced photocatalytic performance for CR(VI) reduction, phenol degradation, and antibacterial activity. ACS Sustain. Chem. Eng. 5 (11), 10551–10562. https://doi.org/10.1021/acssuschemeng.7b02548.

Raal, A., Meos, A., Hinrikus, T., Heinämäki, J., Romāne, E., Gudienė, V., Jakštas, V., Koshovyi, O., Kovaleva, A., Fursenco, C., Chiru, T., Nguyen, H.T., 2020. Dragendorff's reagent: historical perspectives and current status of a versatile reagent introduced over 150 years ago at the University of Dorpat, Tartu, Estonia. Pharmazie 75 (7), 299–306. https://doi.org/10.1691/ph.2020.0438.

Rahmayanti, M., Nurul Syakina, A., Fatimah, I., Sulistyaningsih, T., 2022. Green synthesis of magnetite nanoparticles using peel extract of jengkol (Archidendron pauciflorum) for methylene blue adsorption from aqueous media. Chem. Phys. Lett. 803, 1–8. https://doi.org/10.1016/j.cplett.2022.139834.

Rasoulzadeh, H., Mohseni-Bandpei, A., Hosseini, M., Safari, M., 2019. Mechanistic investigation of ciprofloxacin recovery by magnetite–imprinted chitosan nanocomposite: isotherm, kinetic, thermodynamic and reusability studies. Int. J. Biol. Macromol. 133, 712–721. https://doi.org/10.1016/j.ijbiomac.2019.04.139.

Rusmana, M.H.G., Sulistyaningsih, T., 2021. Preparation of magnetite-tannin guava leaves as Pb(II) adsorbent. Indonesian J. Chem. Environ. 4 (2), 39–48. https://doi.org/10.21831/ijoce.v4i2.48400.

Saif, S., Tahir, A., Chen, Y., 2016. Green synthesis of iron nanoparticles and their environmental applications and implications. Nanomaterials 6 (11), 1–26. https://doi.org/10.3390/nano6110209.

Sankhalkar, S., Vernekar, V., 2016. Quantitative and qualitative analysis of phenolic and flavonoid content in *Moringa oleifera* Lam and *Ocimum tenuiflorum* L. Pharmacogn. Res. 8 (1), 16–21. https://doi.org/10.4103/0974-8490.171095.

Sebastian, A., Nangia, A., Prasad, M.N.V., 2019. Cadmium and sodium adsorption properties of magnetite nanoparticles synthesized from Hevea brasiliensis Muell. Arg. bark: Relevance in amelioration of metal stress in rice. J. Hazard. Mater. 371 (March 2018), 261–272. https://doi.org/10.1016/j.jhazmat.2019.03.021.

Septiani, N.K.A., Parwata, I.M.O.A., Putra, A.A.B., 2018. Penentuan Kadar Total Fenol, Kadar Total Flavonoid dan Skrining Fitokimia Ekstrak Etanol Daun Gaharu (*Gyrinops versteegii*). Jurnal Matematika, Sains, Dan Pembelajarannya 12 (1), 78–89.

Stan, M., Lung, I., Soran, M.L., Opris, O., Leostean, C., Popa, A., Copaciu, F., Lazar, M.D., Kacso, I., Silipas, T.D., Porav, A.S., 2019. Data on the removal of Optilan Blue dye from aqueous media using starch-coated green synthesized magnetite nanoparticles. Data Brief 25. https://doi.org/10.1016/j.dib.2019.104165.

Sulistyaningsih, T., Silalahi, D.S.V., Santosa, S.J., Siswanta, D., Rusdiarso, B., 2013. Synthesis and characterization of magnetic MgAl-NO_3-HT composite via the chemical co-precipitation method. Int. Conf. Biol. Environ. Chem. IPCBEE 58 (19), 95–99. https://doi.org/10.7763/IPCBEE.

Sulistyaningsih, T., Santosa, S.J., Siswanta, D., Rusdiarso, B., 2016. Adsorption of [AuCl4]– on ultrasonically and mechanical-stirring assisted Mg/Al-NO3 hydrotalcite-magnetite. Indonesian J. Chem. 16 (3), 268–276. https://doi.org/10.22146/IJC.21141.

Sulistyaningsih, T., Santosa, S.J., Siswanta, D., Rusdiarso, B., 2017. Synthesis and characterization of magnetites obtained from mechanically and sonochemically assissted Co-precipitation and reverse Co-precipitation methods. Int. J. Mater. Mech. Manuf. 5 (1), 16–19. https://doi.org/10.18178/ijmmm.2017.5.1.280.

Sulistyaningsih, T., Ariyani, S., Astuti, W., 2021. Preparation of magnetite coated humic acid (Fe_3O_4-HA) as malachite green dye adsorbent. J. Phys. Conf. Ser. 1918 (3) https://doi.org/10.1088/1742-6596/1918/3/032005.

Tamoradi, T., Mousavi, S.M., 2020. In situ biogenic synthesis of functionalized magnetic nanoparticles with Ni complex by using a plant extract (Pistachio leaf) and its catalytic evaluation towards polyhydroquinoline derivatives in green conditions. Polyhedron 175, 1–23. https://doi.org/10.1016/j.poly.2019.114211.

Tones, A.R.M., Eyng, E., Zeferino, C.L., Ferreira, S.de O., Alves, A.A.de A., Fagundes-Klen, M.R., Sehn, E., 2020. Spectral deconvolution associated to the Gaussian fit as a tool for the optimization of photovoltaic electrocoagulation applied in the treatment of textile dyes. Sci. Total Environ. 713, 136301 https://doi.org/10.1016/j.scitotenv.2019.136301.

Uddin, M.K., Baig, U., 2019. Synthesis of Co_3O_4 nanoparticles and their performance towards methyl orange dye removal: characterisation, adsorption and response surface methodology. J. Clean. Prod. 211, 1141–1153. https://doi.org/10.1016/j.jclepro.2018.11.232.

Zulaicha, A.S., Saputra, I.S., Sari, I.P., Annas, D., 2020. Synthesis and characterization of modified magnetite microparticles (Fe_3O_4) in rust utilization with leaf extract of grass (Imperata cylindrica L). Jurnal Jejaring Matematika Dan Sains 2 (2), 51–55.